## Tunable Interlayer Coupling and Defects-Mediated Magnetic Ordersm\_in MnBi<sub>2</sub>Te<sub>4</sub>-Bi<sub>2</sub>Te<sub>3</sub> Topological Heterostructures

Xiong Yao, <sup>1, 2,\*,#</sup> Qirui Cui, <sup>2, 3,\*</sup> Zengle Huang, <sup>4</sup> Xiaoyu Yuan, <sup>4</sup> Hee Taek Yi, <sup>4</sup> Deepti Jain, <sup>4</sup> Kim Kisslinger, <sup>5</sup> Myung-Geun Han, <sup>5</sup> Weida Wu, <sup>4</sup> Hongxin Yang, <sup>3,#</sup> and Seongshik Oh<sup>1,#</sup>

<sup>1</sup>Center for Quantum Materials Synthesis and Department of Physics & Astronomy, Rutgers, The State University of New Jersey, Piscataway, New Jersey 08854, United States

<sup>2</sup> Ningbo Institute of Materials Technology and Engineering, Chinese Academy of Sciences, Ningbo 315201, China

<sup>3</sup> National Laboratory of Solid State Microstructures, School of Physics, Collaborative Innovation Center of Advanced Microstructures, Nanjing University, Nanjing 210093, China

<sup>4</sup>Department of Physics & Astronomy, Rutgers, The State University of New Jersey, Piscataway, New Jersey 08854, United States

<sup>5</sup> Condensed Matter Physics and Materials Science, Brookhaven National Laboratory, Upton, New York 11973, United States

\* Xiong Yao and Qirui Cui contributed equally to this work

\*Email: xiong.yao@rutgers.edu, hongxin.yang@nju.edu.cn, ohsean@physics.rutgers.edu

Formatted: Font: +Body (Calibri)

Formatted: Normal

## Abstract

The natural van der Waals superlattice MnBi<sub>2</sub>Te<sub>4</sub> and its derived (MnBi<sub>2</sub>Te<sub>4</sub>)<sub>n</sub>(Bi<sub>2</sub>Te<sub>3</sub>)<sub>m</sub> compounds provide an optimalideal platform to combine topology and magnetism in one system with minimal<del>significantly reduced</del> structural disorder. The realization of quantum anomalous Hall effect in this system favors ferromagnetic ground state, which is challenging considering that the Mn-Mn interlayer coupling in MnBi<sub>2</sub>Te<sub>4</sub> is antiferromagnetic. Here we demonstrate that the sign and magnitude of the interlayer coupling demonstrate the manipulation of ferromagnetic and antiferromagnetic in the interlayer coupling in MnBi<sub>2</sub>Te<sub>4</sub>-Bi<sub>2</sub>Te<sub>3</sub> heterostructures can be controlled not only by the interlayer distance between the two Mn layers but also by parameters outside the Mn-Mn layers, based on systematic transport measurements and first principles calculations. We show that the presence of ferromagnetism can be induced by slight MnBi antisite defects outside the Mn-Mn layer can convert in MnBi<sub>2</sub>Te<sub>4</sub> layers the sign of interlayer magnetic coupling, from antiferromagnetic to ferromagnetic or vice versa, depending on their density. The presence of Additional-Bi<sub>2</sub>Te<sub>3</sub> dilution layers outside the two MnBi<sub>2</sub>Te<sub>4</sub> septuple layers at the top and bottom of the heterostructures also strongly affects the strength of the magnetic ean be used as the knob to mediate the magnetic interlayer coupling, interlayer coupling. Our results highlight that e multitude of tuning parameters that can be utilized toward effetunable topological quantum materials and devices based on this highlight new approaches to control the magnetic interlayer coupling in-MnBi<sub>2</sub>Te<sub>4</sub>-Bi<sub>2</sub>Te<sub>3</sub> heterostructures-films, shedding light on the realization of tunable .quantum phenomena as well as topological spintronic applications.

 $\label{eq:Keywords: Magnetic topological insulator, Interlayer coupling, $MnBi_2Te_4$, Magnetic defects, Tunable magnetism}$ 

Intrinsic magnetic topological insulators (MTIs) such as the MnBi<sub>2</sub>Te<sub>4</sub>(Bi<sub>2</sub>Te<sub>3</sub>)<sub>n</sub> (n = 0, 1, 2, ...) compounds, as the natural stacking of stoichiometric van der Waals units, incorporate topological states and magnetism in a manner that introduces significantly less structural disorder than magnetic doping[1-6]. The experimental demonstration of quantum anomalous Hall effect (QAHE) and robust axion insulator state in MnBi<sub>2</sub>Te<sub>4</sub> compound[2,3,7] highlights its potentials of being exploited in topological spintronics. The MnBi<sub>2</sub>Te<sub>4</sub> layers are ferromagnetically coupled within each septuple layer (SL) and antiferromagnetically coupled between SLs in A-type configuration[8]. The realization of QAHE requires spontaneous magnetization at zero magnetic field, which means ferromagnetic (FM) states are preferable for realistic applications[2,5,9,10].

In the MnBi<sub>2</sub>Te<sub>4</sub>(Bi<sub>2</sub>Te<sub>3</sub>)<sub>n</sub> bulk crystals, the antiferromagnetic (AFM) interlayer coupling becomes weaker and eventually turns into FM as n increases, owing to the increased interlayer Mn-Mn distance by intercalation of non-magnetic Bi<sub>2</sub>Te<sub>3</sub> quintuple layers (QLs)[11-13]. Along this approach people successfully synthesized MnBi<sub>4</sub>Te<sub>7</sub>, MnBi<sub>6</sub>Te<sub>10</sub> and MnBi<sub>8</sub>Te<sub>13</sub> bulk crystals[11-14], in which AFM coupling are weakened or even FM phase can be produced. However, the introduction of Bi<sub>2</sub>Te<sub>3</sub> extra spacer layers inevitably leads to diluted overall Mn concentration in MnBi<sub>2</sub>Te<sub>4</sub>(Bi<sub>2</sub>Te<sub>3</sub>)<sub>n</sub>, possibly causing a "dilution effect" on the magnetic properties, similar to the Cr concentration dependent magnetism in Cr-doped (Bi,Sb)<sub>2</sub>Te<sub>3</sub> thin films[15]. The exact role of such "dilution effect" could mix with the influence of Mn-Mn interlayer distance in the study of MnBi<sub>4</sub>Te<sub>7</sub>, MnBi<sub>6</sub>Te<sub>10</sub> and MnBi<sub>8</sub>Te<sub>13</sub> bulk crystals[11-13], thus still remains elusive. On the other hand, recent studies report that magnetic defects such as Mn antisites can induce ferromagnetism in the bulk crystals of MnSb<sub>2</sub>Te<sub>4</sub>[16-20], the sister compound of MnBi<sub>2</sub>Te<sub>4</sub>. Reflective magnetic circular dichroism spectroscopy reveals that Mn-Bi site mixing also modifies or even changes the sign of magnetic interactions in MnBi<sub>4</sub>Te<sub>7</sub> and MnBi<sub>6</sub>Te<sub>10</sub>

compounds[17]. Manipulating the ferromagnetism in these materials in a controllable manner is desirable for potential spintronic applications.

In order to investigate the Mn dilution effect in MnBi<sub>2</sub>Te<sub>4</sub>-Bi<sub>2</sub>Te<sub>3</sub> heterostructures, we designed the sample structures shown in Fig. 1(a), in which the top and bottom additional n QL Bi<sub>2</sub>Te<sub>3</sub> can be regarded as "dilution layers". With increasing n, the overall Mn concentration reduces as the film becomes thicker while the Mn interlayer distance remains unchanged, so that we can extract the influence of dilution effect separately. However, in bulk crystals, it is difficult to However, due to thermodynamic limitations during the growth process, controlling the stacking sequence and repeating number of MnBi<sub>2</sub>Te<sub>4</sub> and Bi<sub>2</sub>Te<sub>3</sub> layers, in a desired form are difficult due to thermodynamic limitations during the growth process in bulk crystals. On the other hand, with the layer-by-layer molecular beam epitaxy (MBE) technique, it is Owing to the enhanced controllability possible to achieve the desired of the layer by layer growth mode, the stacking of MnBi<sub>2</sub>Te<sub>4</sub> and Bi<sub>2</sub>Te<sub>3</sub> layers at the atomic level can be flexibly controlled by molecular beam epitaxy (MBE)[21-25]. We grew samples with varying n values on 10 mm × 10 mm Al<sub>2</sub>O<sub>3</sub> (0001) substrates using a custom built SVTA MOS-V-2 MBE system with base pressure of low 10<sup>-10</sup> Torr. Substrates were cleaned ex situ by 5 minutes exposure to UV-generated ozone and in situ by heating to 750 °C under oxygen pressure of  $1 \times 10^{-6}$  Torr for 10 minutes. The substrate temperature was then cooled down to 300 °C for the deposition of MnBi<sub>2</sub>Te<sub>4</sub> and Bi<sub>2</sub>Te<sub>3</sub> layers. Between the deposition of each SL MnBi<sub>2</sub>Te<sub>4</sub> or each QL Bi<sub>2</sub>Te<sub>3</sub> layer, we annealed the film at 300 °C for 1 minute under Te flux. Then Te capping layer was deposited on top after the samples were cooled down to room temperature. Fig. 1(b) shows the high-angle annular dark-field scanning transmission electron microscopy (HAADF-STEM) image of a MnBi<sub>2</sub>Te<sub>4</sub>-Bi<sub>2</sub>Te<sub>3</sub> heterostructure with n = 2, which exhibits well-defined QL and SL structures of Bi<sub>2</sub>Te<sub>3</sub> and MnBi<sub>2</sub>Te<sub>4</sub> layers, respectively, with sharp van der Waals gaps between two adjacent layers. Even though the very bottom Bi<sub>2</sub>Te<sub>3</sub> layer was buried into the Al<sub>2</sub>O<sub>3</sub> substrate, the outline of this layer can still be recognized by the contrast difference. The sample quality was further confirmed by reflection high-energy electron diffraction (RHEED) patterns, as shown in Fig. 1(c). The patterns were taken after the deposition of all the Bi<sub>2</sub>Te<sub>3</sub> and MnBi<sub>2</sub>Te<sub>4</sub> layers. The bright streaky patterns indicate a high-quality epitaxial growth of the heterostructure samples.

Since the top and bottom n QL  $Bi_2Te_3$  layers only increase the film thickness, while keeping the interlayer distance between the two  $MnBi_2Te_4$  layers constant, and lead to a "diluted" overall

Mn concentration in the heterostructures, we define these extra Bi<sub>2</sub>Te<sub>3</sub> layers as "dilution layers". To investigate the exact role that these dilution layers play in the magnetic properties of MnBi<sub>2</sub>Te<sub>4</sub>-Bi<sub>2</sub>Te<sub>3</sub> heterostructures, we performed systematic longitudinal and Hall resistance measurements on these samples. All measurements were performed using the standard van der Pauw geometry, by manually pressing four indium wires on the corners of each sample. Raw data of  $R_{xx}$  and  $R_{xy}$ were properly symmetrized and anti-symmetrized. Fig. 2(a) gives the temperature dependent longitudinal sheet resistance for heterostructures with n from 0 to 5. A semiconducting trend was observed in n = 0 and n = 1 samples, then transitions to a metallic trend in samples with larger n values. An upturn behavior appears at low temperatures for all the samples. This upturn behavior is commonly observed in ferromagnetic topological insulators [15,21,26-28], in contrast with the previously reported antiferromagnetic peaks on the Rxx-T curves of MnBi<sub>2</sub>Te<sub>4</sub>(Bi<sub>2</sub>Te<sub>3</sub>)<sub>n</sub> thin flakes[2,3,11]. The origin of this upturn behavior is related to the ferromagnetic ordering induced by Mn<sub>Bi</sub> antisites in MnBi<sub>2</sub>Te<sub>4</sub> layers, which will be discussed below. The arrows in Fig. 2(a) mark the upturn temperature of each sample, which we denote as T<sub>O</sub>. Fig. 2(a) demonstrates a monotonic decrease of To with increasing Bi<sub>2</sub>Te<sub>3</sub> dilution layers, indicating gradually weakened ferromagnetism.

Fig. 2(b) exhibits the corresponding magnetic field dependent longitudinal resistance for all the samples measured at 2 K. There are several peculiar features worth mentioning in Fig. 2(b). First, in samples n = 0, 1, 2 we can obviously observe two symmetric shoulder peaks at around 3 T, which are absent in samples n = 3, 4, 5. This shoulder feature is commonly observed in MnBi<sub>2</sub>Te<sub>4</sub> and is related to magnetic-field-driven spin-flipping antiferromagneantiferromagnet [3], suggesting the presence of AFM phase in samples n = 0, 1, 2. As marked by the dash lines in Fig. 2(b), the characteristic magnetic field of shoulder feature remains unchanged for samples n = 0, 1 and 2, but the intensity of the shoulder features gradually reduces as n increases then completely vanishes in samples n = 3, 4 and 5, indicating the AFM coupling is reduced by adding Bi<sub>2</sub>Te<sub>3</sub> dilution layers. Second, all the curves exhibit clear negative magnetoresistance (MR) peaks around zero field with hysteresis in samples n = 0 and 1, which are generally observed in various FM materials and regarded as features of FM phase [2,21]. With increasing Bi<sub>2</sub>Te<sub>3</sub> dilution layers, the intensity of zero field peaks reduces and the hysteresis feature smears out, indicating weakened FM coupling.

The anomalous Hall effect is another probe to detect the magnetic signatures in thin film samples. We conducted Hall resistance measurements on all samples and the data are shown in Fig. 3(a). It should be noted that all the samples exhibit hysteresis loops at the low field range, which are solid evidence of net magnetization resulting from ferromagnetism. As a result of increasing the number of Bi<sub>2</sub>Te<sub>3</sub> dilution layers, the Hall loops monotonically shrinks in Fig. 3(a), reflecting weakened FM coupling. As mentioned above, the upturn behavior in  $R_{xx}$  vs T, the zero field peaks in MR curves, together with the Hall hysteresis loops all support the existence of FM phase in our heterostructure samples. To clearly demonstrate the influence of Bi<sub>2</sub>Te<sub>3</sub> dilution layers in the systematic evolution of ferromagnetism, we summarize the coercive fields  $H_C$  of each sample together with the upturn temperature T<sub>0</sub> in Fig. 3(b).  $H_C$  and T<sub>0</sub> follows very similar trend of monotonic drop with thicker dilution layers, suggesting that reflecting the underlying origin should be the same. To sSummarizinge the transport results in Fig. 2 and Fig. 3, AFM and FM phase coexist in our samples and the magnetic coupling of both phases become weaker with addedby adding Bi<sub>2</sub>Te<sub>3</sub> dilution layers.

Considering the AFM nature of  $MnBi_2Te_4$  and  $MnBi_4Te_7$  compounds, the origin of FM phase should be discussed here. Magnetic defects like Mn antisites or Mn-Bi site mixing are reported to produce FM phase in  $MnSb_2Te_4$ ,  $MnBi_4Te_7$  and  $MnBi_6Te_{10}$  [16-20]. To determine the distribution of magnetic defects in our samples, we mapped out the  $MnBi_4$  antisite defects in a heterostructure sample with n=0 by atomic resolution scanning tunneling microscopy (STM) imaging (Fig. 3(c)). The  $MnBi_4$  antisites appear as dark defects in the marked triagonal circles. The density of  $MnBi_4$  antisites are determined as 2.1% on average by counting the defects in the measured region in Fig. 3(c), while the distribution of Mn is rather inhomogeneous as the density in Mn clustered regions are obviously higher than other regions. People might suspect that the weakened magnetic coupling (both FM and AFM) is related to the Mn diffusion in  $Bi_2Te_3$  dilution layers. To rule out this possibility, we conducted STM imaging of Mn concentration in a control sample with n=4 (Fig. 3(d)). The Mn density ( $\sim$ 0.2%) is more than one order lower than the value in Fig. 3(c), strongly suggesting the  $MnBi_4$  antisite defects are mostly confined within the  $MnBi_2Te_4$  layer and the interlayer Mn diffusion, if any, is minuscule compared with the Mn density in  $MnBi_2Te_4$  layer.

To examine the exact role that the magnetic defects play in the magnetism of our heterostructures, we performed first-principles calculations with the Vienna ab initio simulation package (VASP) based on the density functional theory (DFT). The exchange-correlation functionals are treated by the generalized gradient approximation (GGA) in Perdew-Burke-Ernzerhof (PBE) form. The cutoff energy of plane wave expansion is set to 420 eV. An 18×18×1 Γ-center k-point mesh is dense enough for sampling the Brillouin zone. A vacuum space of 15 Å is adopted in periodical direction for avoiding the interactions between adjacent layers. All structures are fully relaxed until Hellmann-Feynman force acting on each atom is less than 10<sup>-2</sup> eV/Å, and the convergence criterion of total energy is set to 10<sup>-6</sup> eV. For describing the strong correlation effects of 3d electrons of Mn, GGA+U method is adopted where the Ueff is set to 3 eV. The effect of van der Waals interactions are considered by employing the DFT+D3 method.

Since the exact location and distribution of Mn atoms in MnBi<sub>2</sub>Te<sub>4</sub> layer are unclear, we proposed one possible configuration for Mn substitutions in the left panel of Fig. 4(a), where the mixed color represents Bi atoms substituted by Mn atoms. We conducted first-principles calculations on this configuration to demonstrate the influence of Mn defects. As indicated in Fig. 4(a), the ground state of the MnBi<sub>2</sub>Te<sub>4</sub>-Bi<sub>2</sub>Te<sub>3</sub> heterostructure without Mn substitution was determined as AFM. As more Bi sites are replaced by Mn atoms, the energy difference between AFM and FM coupling quickly narrows to nearly 0 at the critical Mn doping level of 3.57% and FM coupling becomes the ground state, then the FM order experiences a peak strength at 7.14% Mn before reducing again. It is worth noting that the AFM coupling would become the ground state again at above 14.28% Mn doping according to the trend in Fig. 4(a), which is consistent with the observations in MnTe intercalated MnBi<sub>2</sub>Te<sub>4</sub> superlattices [25]. Even though Fig. 4(a) only gives one possible configuration for Mn substitution, we believe the trend shown in Fig. 4(a) depicts a general picture for all possible Mn locations, which means there is a critical Mn density that determines the magnetic ground state. As observed in Fig. 3(c), the distribution of Mn concentration is obviously inhomogeneous in our films, suggesting the Mn density could be lower than the critical density at Mn poor regions but higher than that value at Mn clustered regions. As a result, the magnetic exchange interaction also shows the same inhomogeneity, causing the coexistence of FM and AFM phases. The Mn inhomogeneity controlled magnetic ground states give a consistent interpretation of the transport measurement results on our samples.

Next, we focus on the influence of Bi<sub>2</sub>Te<sub>3</sub> dilution layers in our samples. To understand the dilution layer tunable interlayer coupling, we carried out first-principles calculations to investigate the exact role of Bi<sub>2</sub>Te<sub>3</sub> dilution layers. As shown in Fig. 4(b) and (c), the magnitude

of energy difference between interlayer AFM and FM phases continuously decreases from 0.075 to 0.051 meV with increasing Bi<sub>2</sub>Te<sub>3</sub> dilution layer thickness. Adding Bi<sub>2</sub>Te<sub>3</sub> dilution layers shifts up the Fermi level of MnBi<sub>2</sub>Te<sub>4</sub> to the conduction bands, resulting in the occupations of opposite spin-polarized states that breaks the high-spin configuration state S = 5/2, which leads to the decrease of interlayer AFM exchange coupling (Fig. 4(c)). The Aabove DFT results unveil the influence of Bi<sub>2</sub>Te<sub>3</sub> dilution layers on AFM coupling strength, consistent with our experimental observations of AFM shoulder peaks vanishing in n > 2 samples (Fig. 2(b)). To compare the tuning effect of Bi<sub>2</sub>Te<sub>3</sub> dilution layer with Mn interlayer distance, we grew a seriesal of control samples with the same Bi<sub>2</sub>Te<sub>3</sub> thickness but varied Mn interlayer distance (Fig. S1). The summarized Hc and  $T_0$  values show weak dependence on the Mn interlayer distance, implying the Bi<sub>2</sub>Te<sub>3</sub> dilution layer tuning is a more effective manipulation strategy. Our observations suggests prove—that the dilution layer tuning can be a general way to manipulate both AFM and FM coupling in MnBi<sub>2</sub>Te<sub>4</sub>-Bi<sub>2</sub>Te<sub>3</sub> heterostructures.

In summary, we observed coexisting AFM and FM phases in our MnBi<sub>2</sub>Te<sub>4</sub>-Bi<sub>2</sub>Te<sub>3</sub> heterostructures based on transport measurements, which could attribute to the Mn substitution in MnBi<sub>2</sub>Te<sub>4</sub> layer. First-principles calculations and STM imaging suggestadvise that the inhomogeneous distribution of Mn<sub>Bi</sub> defects is the decisive factor that controls the magnetic ground states, providing an intuitive interpretation on the formation of FM phase. Both AFM and FM features that appear on transport results gradually reduce with adding more Bi<sub>2</sub>Te<sub>3</sub> dilution layers, indicating a tunable magnetic interlayer coupling. Our calculations reveal that Bi<sub>2</sub>Te<sub>3</sub> dilution layers could shift the Fermi level and resulting in the occupationy of opposite spin-polarized states, leading to reduced AFM exchange coupling. Our work demonstrates that intentional Bi<sub>2</sub>Te<sub>3</sub> dilution layers can be used as an effective tool to control tuning can be an effective knob to manipulate the magnetic properties in topological MnBi<sub>2</sub>Te<sub>4</sub>-Bi<sub>2</sub>Te<sub>3</sub> thin films, which toward is insightful for growing novel FM MnBi<sub>2</sub>Te<sub>4</sub> materials to realize high temperature QAHE and other designing topological spintronic effects devices.

Acknowledgment.—The work at Rutgers is supported by National Science Foundation's DMR2004125, Army Research Office's W911NF2010108, MURI W911NF2020166, and the center for Quantum Materials Synthesis (cQMS), funded by the Gordon and Betty Moore Foundation's EPiOS initiative through grant GBMF10104. The work at Ningbo Institute of

Materials Technology and Engineering is supported by. The work at Nanjing University is supported by.

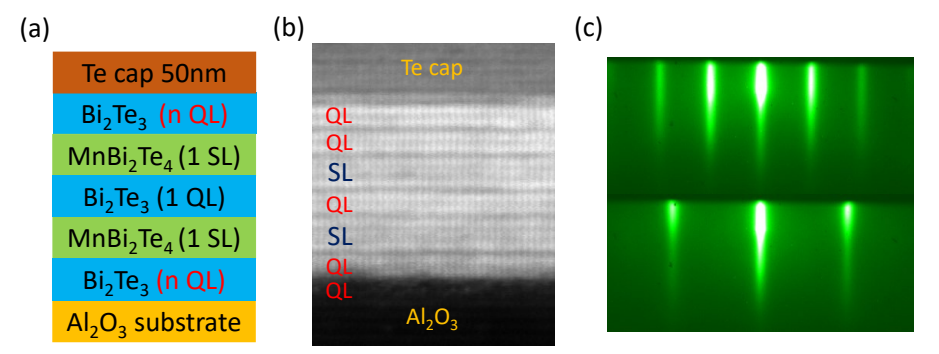


FIG.1. (a) Illustration of the  $MnBi_2Te_4$ - $Bi_2Te_3$  heterostructures. (b) High-angle annular dark-field scanning transmission electron microscopy (HAADF-STEM) image of a heterostructure sample with n=2. The stacking of  $MnBi_2Te_4$  and  $Bi_2Te_3$  layers are labeled by SL and QL, respectively. (c) Reflection high-energy electron diffraction (RHEED) patterns of the as—grown  $MnBi_2Te_4$ - $Bi_2Te_3$  heterostructure at two high symmetry directions.

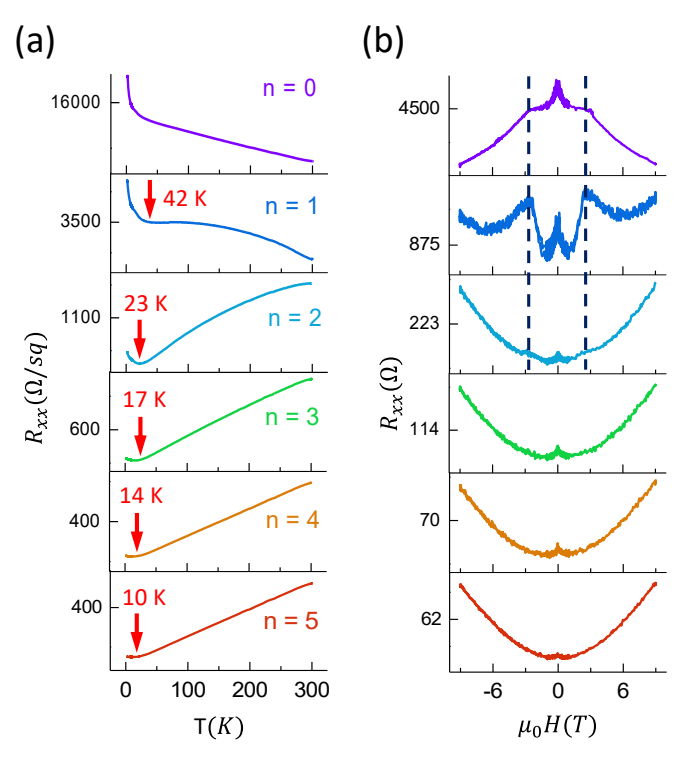


FIG.2. (a) Temperature-dependent longitudinal sheet resistance of the  $MnBi_2Te_4$ - $Bi_2Te_3$  heterostructures with n values from 0 to 5. (b) The corresponding magnetic field dependent longitudinal resistance of the same samples measured at 2 K.

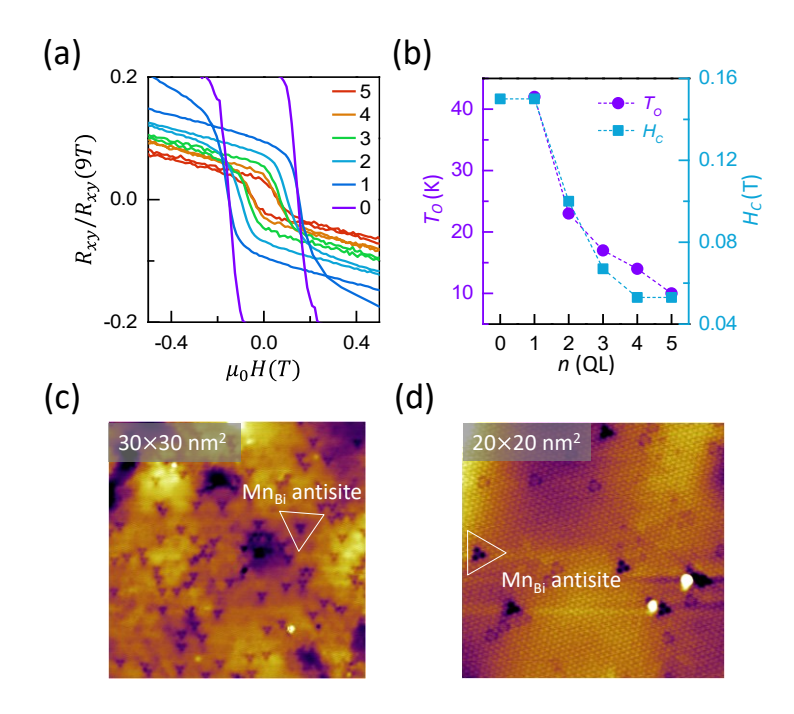


FIG.3. (a) Normalized Hall resistance of the  $MnBi_2Te_4$ - $Bi_2Te_3$  heterostructures with n values from 0 to 5 measured at 2 K. (b) Summary of ferromagnetic ordering temperatures  $T_O$  determined by Fig. 2a and coercive fields  $H_C$  determined by Fig. 3a. (c, d) Atomic resolution scanning tunneling microscopy (STM) imaging of the  $MnBi_2Te_4$ - $Bi_2Te_3$  heterostructures with (c) n=0 and (d) n=4.

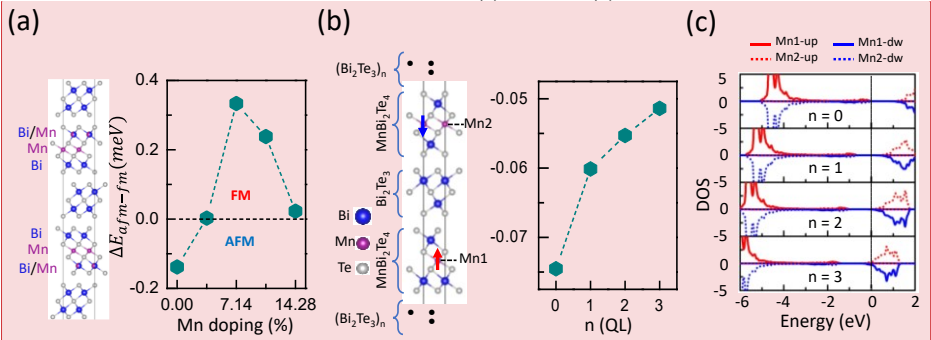


FIG.4. (a) Left panel is the schematic structure of one possible Mn doping configuration in MnBi<sub>2</sub>Te<sub>4</sub>-Bi<sub>2</sub>Te<sub>3</sub> heterostructures. Right panel shows the Mn doping level dependent energy difference between AFM and FM ground states obtained by first principles calculations. (b) Left panel is the schematic structure of the MnBi<sub>2</sub>Te<sub>4</sub>-Bi<sub>2</sub>Te<sub>3</sub> heterostructures with varying Bi<sub>2</sub>Te<sub>3</sub> dilution layers. Right panel shows the dilution layer thickness dependent energy difference between AFM and FM ground states obtained by first principles calculations. (c) Spin-polarized density of states for Mn atoms. The Fermi level is obviously shifted up when the Bi<sub>2</sub>Te<sub>3</sub> dilution layers increase.

**Commented [S01]:** In the right figure of (b), label for the vertical axis is missing.

## REFERENCES

- [1]E. D. L. Rienks, S. Wimmer, J. Sanchez-Barriga, O. Caha, P. S. Mandal, J. Ruzicka, A. Ney, H. Steiner, V. V. Volobuev, H. Groiss, M. Albu, G. Kothleitner, J. Michalicka, S. A. Khan, J. Minar, H. Ebert, G. Bauer, F. Freyse, A. Varykhalov, O. Rader, and G. Springholz, Large magnetic gap at the Dirac point in Bi2Te3/MnBi2Te4 heterostructures, Nature **576**, 423-428 (2019).
- [2]Y. Deng, Y. Yu, M. Z. Shi, Z. Guo, Z. Xu, J. Wang, X. H. Chen and Y. Zhang, Quantum anomalous Hall effect in intrinsic magnetic topological insulator MnBi2Te4, Science **367**, 895-900 (2020).
- [3]C. Liu, Y. Wang, H. Li, Y. Wu, Y. Li, J. Li, K. He, Y. Xu, J. Zhang and Y. Wang, Robust axion insulator and Chern insulator phases in a two-dimensional antiferromagnetic topological insulator, Nat. Mater. **19**, 522-527 (2020).
- [4]Y. J. Chen, L. X. Xu, J. H. Li, Y. W. Li, H. Y. Wang, C. F. Zhang, H. Li, Y. Wu, A. J. Liang, C. Chen, S. W. Jung, C. Cacho, Y. H. Mao, S. Liu, M. X. Wang, Y. F. Guo, Y. Xu, Z. K. Liu, L. X. Yang, and Y. L. Chen, Topological Electronic Structure and Its Temperature Evolution in Antiferromagnetic Topological Insulator MnBi2Te4, Physical Review X 9, 041040 (2019).
- [5]J. Li, Y. Li, S. Du, Z. Wang, B. L. Gu, S. C. Zhang, K. He, W. Duan and Y. Xu, Intrinsic magnetic topological insulators in van der Waals layered MnBi2Te4-family materials, Sci. Adv. 5, eaaw5685 (2019).
- [6]X. Yao, B. Gao, M. G. Han, D. Jain, J. Moon, J. W. Kim, Y. Zhu, S. W. Cheong and S. Oh, Record High-Proximity-Induced Anomalous Hall Effect in (BixSb1-x)2Te3 Thin Film Grown on CrGeTe3 Substrate, Nano Lett. 19, 4567-4573 (2019).
- [7]D. Zhang, M. Shi, T. Zhu, D. Xing, H. Zhang and J. Wang, Topological Axion States in the Magnetic Insulator MnBi2Te4 with the Quantized Magnetoelectric Effect, Phys. Rev. Lett. **122**, 206401 (2019). [8]P. M. Sass, J. Kim, D. Vanderbilt, J. Yan and W. Wu, Robust A-Type Order and Spin-Flop Transition on the Surface of the Antiferromagnetic Topological Insulator MnBi2Te4, Phys. Rev. Lett. **125**, 037201 (2020).
- [9]J. Cui, B. Lei, M. Shi, Z. Xiang, T. Wu and X. Chen, Layer-Dependent Magnetic Structure and Anomalous Hall Effect in the Magnetic Topological Insulator MnBi4Te7, Nano Lett. **23**, 1652-1658 (2023).
- [10]M. M. Otrokov, I. P. Rusinov, M. Blanco-Rey, M. Hoffmann, A. Y. Vyazovskaya, S. V. Eremeev, A. Ernst, P. M. Echenique, A. Arnau and E. V. Chulkov, Unique Thickness-Dependent Properties of the van der Waals Interlayer Antiferromagnet MnBi2Te4 Films, Phys. Rev. Lett. **122**, 107202 (2019).
- [11]C. Hu, K. N. Gordon, P. Liu, J. Liu, X. Zhou, P. Hao, D. Narayan, E. Emmanouilidou, H. Sun, Y. Liu, H. Brawer, A. P. Ramirez, L. Ding, H. Cao, Q. Liu, D. Dessau, and N. Ni, A van der Waals antiferromagnetic topological insulator with weak interlayer magnetic coupling, Nat. Commun. **11**, 97 (2020).
- [12]J. Wu, F. Liu, M. Sasase, K. Ienaga, Y. Obata, R. Yukawa, K. Horiba, H. Kumigashira, S. Okuma, T. Inoshita, and H. Hosono, Natural van der Waals heterostructural single crystals with both magnetic and topological properties, Sci. Adv. 5, eaax9989 (2019).
- [13]C. Hu, L. Ding, K. N. Gordon, B. Ghosh, H. J. Tien, H. Li, A. G. Linn, S. W. Lien, C. Y. Huang, S. Mackey, J. Liu, P. V. S. Reddy, B. Singh, A. Agarwal, A. Bansil, M. Song, D. Li, S. Y. Xu, H. Lin, H. Cao, T. R. Chang, D. Dessau, and N. Ni, Realization of an intrinsic ferromagnetic topological state in MnBi8Te13, Sci. Adv. 6, eaba4275 (2020).
- [14]X. Wu, J. Li, X.-M. Ma, Y. Zhang, Y. Liu, C.-S. Zhou, J. Shao, Q. Wang, Y.-J. Hao, Y. Feng, E. F. Schwier, S. Kumar, H. Sun, P. Liu, K. Shimada, K. Miyamoto, T. Okuda, K. Wang, M. Xie, C. Chen, Q. Liu, C. Liu, and Y. Zhao, Distinct Topological Surface States on the Two Terminations of MnBi4Te7, Physical Review X 10, 031013 (2020).
- [15]Y. Ou, C. Liu, L. Zhang, Y. Feng, G. Jiang, D. Zhao, Y. Zang, Q. Zhang, L. Gu, Y. Wang, K. He, X. Ma, and Q.-K. Xue, Heavily Cr-doped (Bi,Sb)2Te3 as a ferromagnetic insulator with electrically tunable conductivity, APL Materials **4**, 086101 (2016).

[16]F. Islam, Y. Lee, D. M. Pajerowski, J. Oh, W. Tian, L. Zhou, J. Yan, L. Ke, R. J. McQueeney and D. Vaknin, Role of Magnetic Defects in Tuning Ground States of Magnetic Topological Insulators, Adv. Mater. **35**, e2209951 (2023).

[17]X. Xu, S. Yang, H. Wang, R. Guzman, Y. Gao, Y. Zhu, Y. Peng, Z. Zang, M. Xi, S. Tian, Y. Li, H. Lei, Z. Luo, J. Yang, Y. Wang, T. Xia, W. Zhou, Y. Huang, and Y. Ye, Ferromagnetic-antiferromagnetic coexisting ground state and exchange bias effects in MnBi4Te7 and MnBi6Te10, Nat. Commun. 13, 7646 (2022). [18]Y. Liu, L.-L. Wang, Q. Zheng, Z. Huang, X. Wang, M. Chi, Y. Wu, B. C. Chakoumakos, M. A. McGuire, B. C. Sales, W. Wu, and J. Yan, Site Mixing for Engineering Magnetic Topological Insulators, Physical Review X 11, 021033 (2021).

[19]C. Hu, S.-W. Lien, E. Feng, S. Mackey, H.-J. Tien, I. I. Mazin, H. Cao, T.-R. Chang and N. Ni, Tuning magnetism and band topology through antisite defects in Sb-doped MnBi4Te7, Phys. Rev. B **104** (2021). [20]Z. Zang, Y. Zhu, M. Xi, S. Tian, T. Wang, P. Gu, Y. Peng, S. Yang, X. Xu, Y. Li, B. Han, L. Liu, Y. Wang, P. Gao, J. Yang, H. Lei, Y. Huang, and Y. Ye, Layer-Number-Dependent Antiferromagnetic and Ferromagnetic Behavior in MnSb2Te4, Phys. Rev. Lett. **128**, 017201 (2022).

[21]X. Yao, H. T. Yi, D. Jain, M. G. Han and S. Oh, Spacer-Layer-Tunable Magnetism and High-Field Topological Hall Effect in Topological Insulator Heterostructures, Nano Lett. **21**, 5914-5919 (2021). [22]A. R. Mazza, J. Lapano, H. M. Meyerlii, C. T. Nelson, T. Smith, Y. Y. Pai, K. Noordhoek, B. J. Lawrie, T. R. Charlton, R. G. Moore, T. Z. Ward, M. H. Du, G. Eres, and M. Brahlek, Surface-Driven Evolution of the Anomalous Hall Effect in Magnetic Topological Insulator MnBi2Te4 Thin Films, Adv. Funct. Mater. **32** (2022)

[23]T. Hirahara, M. M. Otrokov, T. T. Sasaki, K. Sumida, Y. Tomohiro, S. Kusaka, Y. Okuyama, S. Ichinokura, M. Kobayashi, Y. Takeda, K. Amemiya, T. Shirasawa, S. Ideta, K. Miyamoto, K. Tanaka, S. Kuroda, T. Okuda, K. Hono, S. V. Eremeev, and E. V. Chulkov, Fabrication of a novel magnetic topological heterostructure and temperature evolution of its massive Dirac cone, Nat. Commun. 11, 4821 (2020). [24]J. Lapano, L. Nuckols, A. R. Mazza, Y.-Y. Pai, J. Zhang, B. Lawrie, R. G. Moore, G. Eres, H. N. Lee, M.-H. Du, T. Z. Ward, J. S. Lee, W. J. Weber, Y. Zhang, and M. Brahlek, Adsorption-controlled growth of MnTe(Bi2Te3)n by molecular beam epitaxy exhibiting stoichiometry-controlled magnetism, Phys. Rev. Mater. 4, 111201 (2020).

[25]P. Chen, Q. Yao, J. Xu, Q. Sun, A. J. Grutter, P. Quarterman, P. P. Balakrishnan, C. J. Kinane, A. J. Caruana, S. Langridge, A. Li, B. Achinuq, E. Heppell, Y. Ji, S. Liu, B. Cui, J. Liu, P. Huang, Z. Liu, G. Yu, F. Xiu, T. Hesjedal, J. Zou, X. Han, H. Zhang, Y. Yang, and X. Kou, Tailoring the magnetic exchange interaction in MnBi2Te4 superlattices via the intercalation of ferromagnetic layers, Nature Electronics 6, 18-27 (2023). [26]C. Z. Chang, J. Zhang, X. Feng, J. Shen, Z. Zhang, M. Guo, K. Li, Y. Ou, P. Wei, L. L. Wang, Z. Q. Ji, Y. Feng, S. Ji, X. Chen, J. Jia, X. Dai, Z. Fang, S. C. Zhang, K. He, Y. Wang, L. Lu, X. C. Ma, and Q. K. Xue, Experimental observation of the quantum anomalous Hall effect in a magnetic topological insulator, Science 340, 167-170 (2013).

[27]X. Kou, S. T. Guo, Y. Fan, L. Pan, M. Lang, Y. Jiang, Q. Shao, T. Nie, K. Murata, J. Tang, Y. Wang, L. He, T. K. Lee, W. L. Lee, and K. L. Wang, Scale-invariant quantum anomalous Hall effect in magnetic topological insulators beyond the two-dimensional limit, Phys. Rev. Lett. **113**, 137201 (2014). [28]J. G. Checkelsky, R. Yoshimi, A. Tsukazaki, K. S. Takahashi, Y. Kozuka, J. Falson, M. Kawasaki and Y. Tokura, Trajectory of the anomalous Hall effect towards the quantized state in a ferromagnetic topological insulator, Nat. Phys. **10**, 731-736 (2014).